



Theory of activated glassy relaxation, mobility gradients, surface diffusion, and vitrification in free standing thin films

Stephen Mirigian and Kenneth S. Schweizer

Citation: *The Journal of Chemical Physics* **143**, 244705 (2015); doi: 10.1063/1.4937953

View online: <http://dx.doi.org/10.1063/1.4937953>

View Table of Contents: <http://scitation.aip.org/content/aip/journal/jcp/143/24?ver=pdfcov>

Published by the AIP Publishing

Articles you may be interested in

The effect of a thermal gradient on the electromigration-driven surface morphological stabilization of an epitaxial thin film on a compliant substrate

J. Appl. Phys. **114**, 023503 (2013); 10.1063/1.4812289

Microscopic theory of the glassy dynamics of passive and active network materials

J. Chem. Phys. **138**, 12A521 (2013); 10.1063/1.4773349

Erratum: “Thermodynamics of viscous flow and elasticity of glass forming liquids in the glass transition range”
[*J. Chem. Phys.* **135**, 184501 (2011)]

J. Chem. Phys. **137**, 179902 (2012); 10.1063/1.4766466

Glassy dynamics and mechanical response in dense fluids of soft repulsive spheres. I. Activated relaxation, kinetic vitrification, and fragility

J. Chem. Phys. **134**, 204908 (2011); 10.1063/1.3592563

Thin-film evolution equation for a strained solid film on a deformable substrate: Numerical steady states

J. Appl. Phys. **102**, 073503 (2007); 10.1063/1.2785024

An advertisement for AIP Applied Physics Reviews. On the left, there's a thumbnail image of the journal cover showing a 3D molecular model and some text. To the right, the text "NEW Special Topic Sections" is displayed in large, bold, white letters against a blue background with a molecular model. Below this, the text "NOW ONLINE" is in yellow, followed by "Lithium Niobate Properties and Applications: Reviews of Emerging Trends". At the bottom right, the AIP logo is shown with the text "Applied Physics Reviews".

Theory of activated glassy relaxation, mobility gradients, surface diffusion, and vitrification in free standing thin films

Stephen Mirigian^{a)} and Kenneth S. Schweizer^{a)}

Departments of Materials Science and Chemistry, University of Illinois, Urbana, Illinois 61801, USA

(Received 25 October 2015; accepted 2 December 2015; published online 29 December 2015)

We have constructed a quantitative, force level, statistical mechanical theory for how confinement in free standing thin films introduces a spatial mobility gradient of the alpha relaxation time as a function of temperature, film thickness, and location in the film. The crucial idea is that relaxation speeds up due to the reduction of both near-surface barriers associated with the loss of neighbors in the local cage and the spatial cutoff and dynamical softening near the vapor interface of the spatially longer range collective elasticity cost for large amplitude hopping. These two effects are fundamentally coupled. Quantitative predictions are made for how an apparent glass temperature depends on the film thickness and experimental probe technique, the emergence of a two-step decay and mobile layers in time domain measurements, signatures of confinement in frequency-domain dielectric loss experiments, the dependence of film-averaged relaxation times and dynamic fragility on temperature and film thickness, surface diffusion, and the relationship between kinetic experiments and pseudo-thermodynamic measurements such as ellipsometry. © 2015 AIP Publishing LLC. [<http://dx.doi.org/10.1063/1.4937953>]

I. INTRODUCTION

More than two decades of intense experimental investigation have revealed that geometric confinement can have a large and often puzzling effect on the dynamics of supercooled liquids.^{1–4} This behavior is sensitive to many factors, especially the sample boundary conditions. For free standing thin films, a vapor surface generically speeds up dynamics in the liquid.^{1–3,5–12} This effect is usually attributed to enhanced molecular mobility near the free surface, but it appears to extend to large distances into the film that are well beyond any length scale typically associated with the bulk glass transition.^{2,13,14} While it has long been hoped glassy dynamics under confinement would hold clues about cooperative relaxation in bulk supercooled liquids, this has remained largely unrealized primarily due to complications arising from strong interfacial effects beyond the pure geometric confinement aspect.^{1–4,6,13}

In addition to the fundamental interest, the change of glassy dynamics in thin films is crucial for diverse material applications.^{1,2,15,16} Spatially heterogeneous dynamics in films with a vapor interface are especially important for the fabrication of the so-called “ultra-stable” glasses.^{17,18} An enduring mystery and source of heated discussion and controversy^{1–4} is the apparent breakdown of accepted interrelationships between different experimental probes that hold in the bulk: pseudo-thermodynamic versus dynamic, and time domain versus frequency domain response.^{1,2,5,6,19} It is widely acknowledged that a central question is the nature of the spatial gradient of mobility or alpha relaxation time in the direction orthogonal to the film interface.^{20–22}

To date, a fundamental and comprehensive theoretical understanding remains elusive given the complexity of activated relaxation in bulk supercooled liquids¹³ and the major complications of geometric confinement, interfacial effects and spatial inhomogeneity. Simulations^{23–26} provide valuable insights but cannot access the deeply supercooled regime in thin films (as studied almost exclusively in the laboratory) since they probe only down to temperatures of the order of the dynamic crossover temperature, T_c .^{13,23} Here, the bulk relaxation time is ~8–10 orders of magnitude faster than at T_g , the mobility enhancement at a free surface is only ~3–5 orders of magnitude, and a multi-step alpha relaxation decay of time domain correlation functions (as seen in experiment⁵) is not observed, presumably because spatial mobility gradients are too weak.^{23,25,26} Theoretical progress has been largely phenomenological and relatively modest, with diverse ideas suggested associated with cooperatively re-arranging regions (CRRs²⁷), entropic droplets,²⁸ strings,²⁹ dynamic facilitation,³⁰ and other mechanisms.³¹ Some have even argued that all existing models are at odds with experiment.²² This primitive level of understanding is perhaps unsurprising given the difficulty of formulating a predictive, and thus truly testable, theory of bulk glassy relaxation in globally homogeneous samples.

Very recently, we proposed a quantitative, force-level theory of relaxation in bulk supercooled liquids, the Elastically Collective Nonlinear Langevin Equation (ECNLE) theory,^{32–35} and extended it to free-standing films in order to predict the spatial mobility gradient.³⁶ The key new idea is that vapor interfaces speed up barrier hopping in two distinct but coupled ways by reducing *both* near-surface local caging constraints and spatially long range collective elastic distortion. Predictions for effective vitrification temperatures, dynamic length scales, and mobile layer thicknesses naturally

^{a)}Authors to whom correspondence should be addressed. Electronic addresses: kschweiz@illinois.edu and smirigian@gmail.com.

follow. Our initial results provide a starting point for creating a unified understanding of the central observations of dynamic and pseudo-thermodynamic measurements. The approach can be applied quantitatively to bulk molecular and polymer liquids based on an *a priori* mapping of molecular complexity^{32,34} to an effective hard sphere description using equilibrium equation-of-state (EOS) data.

The goal of this paper is to discuss the recent ECNLE theory for free standing film dynamics in detail and present a wide range of new numerical calculations that systematically address the basic physics of mobility gradients, pseudo-thermodynamic and dynamic measurements of effective glass transition temperatures, and time and frequency dependent correlation functions. Calculations are performed using molecular parameters representative of van der Waals liquids. The goal is not to address any particular chemical system or to fit data, but rather construct a no-adjustable parameter unified understanding of diverse questions relevant to a broad range of different experimental measurements.

Section II reviews bulk ECNLE theory and its extension to free standing films. In a planar film geometry, the activation barrier, and thus the alpha relaxation time, becomes a three-dimensional function of temperature, film thickness, and spatial location. Section III presents systematic model calculations for these dependences. Surface diffusion is briefly considered in Section IV. Time and frequency domain correlation function measurements, including deduced length scales and mobile layers, are studied in Section V. Effective vitrification temperatures are determined in Section VI, and their inter-relationships revealed, which is relevant to diverse experiments such as dye rotation, dielectric relaxation, and ellipsometry. The article concludes in Section VII with a summary and future outlook.

II. THEORY AND MODEL

We first briefly review bulk ECNLE theory with an emphasis on its physical ideas and approximations; technical details are documented in great detail elsewhere.^{32–35} We then discuss its extension to free standing films which was only sketched in our recent communication.³⁶ At its present level of development, ECNLE theory focuses solely on the mean or most probable alpha relaxation time, and does not treat space-time intrinsic dynamic heterogeneity in the bulk. In confinement, this implies films are treated as dynamically homogeneous in the lateral direction.

A. Bulk theory and model mapping

ECNLE theory describes activated relaxation as a mixed local-nonlocal rare event composed of a cage scale large amplitude particle hop or jump which is coupled to a relatively long range, spontaneous, elastic fluctuation needed to sterically accommodate the hop.^{32,33} The cage scale dynamics is described using the NLE evolution equation formulated in terms of the scalar (angularly averaged) particle displacement, $r(t)$, and an effective force felt by a moving particle due to its dynamic surroundings. This force is the

gradient of a microscopic dynamic free energy, $F_{dyn}(r)$, which for a fluid of hard spheres (diameter, d) is

$$\begin{aligned} \beta F_{dyn}(r) = & -3 \ln(r) + \frac{6\phi}{\pi} \int \frac{d\vec{k}}{(2\pi)^3} \frac{C^2(k)S(k)}{1+S^{-1}(k)} \\ & \times \exp\left[-\frac{k^2 r^2}{6}(1+S^{-1}(k))\right] \\ & \equiv F_{id}(r) + F_{cage}(r; \phi). \end{aligned} \quad (1)$$

Here, $\beta = (k_B T)^{-1}$, $\phi \equiv \pi \rho d^3 / 6$ is the fluid volume or packing fraction, $C(k)$ is the direct correlation function in Fourier space, and $S(k) = (1 - \rho C(k))^{-1}$ is the static structure factor. At packing fractions beyond an onset value of $\phi_A \approx 0.43$, the caging term induces transient localization of any tagged particle corresponding to the emergence of a local minimum and maximum of the dynamic free energy. Key features of $F_{dyn}(r)$ include the barrier for *local* cage re-arrangement, F_B , transient localization length, r_{loc} , barrier location, r_B , and jump distance, $\Delta r \equiv r_B - r_{loc} \approx 0.2\text{--}0.4d$ which is an increasing function of packing fraction.

Inspired by phenomenological “elastic models,” especially the so-called “shoving model” of Dyre,³⁷ the large amplitude motion is physically argued to be sterically possible only if there is some small volume expansion or cage dilation of the nearest neighbor shell. This cage expansion requires a relatively long range displacement or strain field emerges in the fluid which implies an additional, spatially nonlocal contribution to the activation barrier. The fluid outside the local cage region can be taken (to good approximation) to be an elastic continuum. Assuming a radially symmetric strain field fluctuation is consistent with the angularly averaged description of particle motion that underlies the NLE approach. From standard elasticity theory, the displacement field is^{33,37}

$$u(r) = \Delta r_{eff} \left(\frac{r_{cage}}{r} \right)^2. \quad (2)$$

Equation (2) applies for distances outside the cage radius, $r > r_{cage} \approx 3d/2$, where r_{cage} is the location of the first minimum of the radial distribution function $g(r)$, and $\Delta r_{eff} \approx 3\Delta r^2/32r_{cage}$ is the orientationally averaged mean cage expansion length which grows with volume fraction or cooling.^{32–34} The barrier associated with the elastic strain field follows by summing over all particle displacements outside the cage region (volume V):

$$\begin{aligned} \beta F_{elastic} &= \int_V d\vec{r} \rho g(\vec{r}) \{ F_{dyn}[r_{loc} + u(\vec{r})] - F_{dyn}[r_{loc}] \} \\ &= \int_V d\vec{r} \rho \frac{1}{2} u(\vec{r})^2 K_0 \\ &= \rho (K_0/2) \int_{r_{cage}}^{\infty} dr 4\pi r^2 u^2(r), \end{aligned} \quad (3)$$

where K_0 is the curvature of the dynamic free energy at its minimum. In the second line, $g(r)$ is set to unity outside the cage (a benign simplification³³) and a harmonic approximation is introduced which is valid since we predict that the cage dilation amplitude is small, $\Delta r_{eff} \leq r_{loc}$. Using Eq. (2) for $u(r)$,

the elastic barrier in the bulk is explicitly given by^{32–34}

$$\beta F_{\text{elastic}} = 12\phi\Delta r_{\text{eff}}^2 r_{\text{cage}}^3 K_0, \quad (4)$$

where all length scales are in units of the particle diameter. The amplitude of the strain field, and hence elastic barrier, is related to the microscopic jump length associated with the local hopping process. Hence, the local and elastic collective barriers are intimately coupled. The growth of the latter barrier plays the central role in the bulk deeply supercooled regime.³⁴

ECNLE theory is rendered quantitatively predictive for real materials by mapping molecules³⁴ or disconnected Kuhn statistical segments for polymers³⁵ to an effective hard sphere fluid guided by the requirement that it exactly reproduces the equilibrium dimensionless density fluctuation amplitude (compressibility) of the liquid,³⁴ $S_0(T) = \rho k_B T \kappa_T$. The latter quantifies the amplitude of nm-scale density fluctuations which is the key order parameter of the theory. Employing the experimental EOS of a specific liquid yields a temperature dependent effective hard sphere packing fraction³⁴

$$\begin{aligned} S_0^{HS} &= \frac{(1-\phi)^4}{(1+2\phi)^2} \equiv S_{0,\text{expt}} \\ &= \rho k_B T \kappa_T = N_s^{-1} \left(-A + \frac{B}{T} \right)^{-2}, \end{aligned} \quad (5)$$

where Percus-Yevick integral equation theory has been used for the thermodynamics and structure of the effective hard sphere fluid, N_s is the number of elementary sites that define a rigid molecule (e.g., $N_s = 6$ for benzene) or Kuhn segment of a polymer ($N_s = 38.4$ for polystyrene (PS)), B is a measure of the liquid cohesive energy, and A is an entropic packing factor. The final relation in Eq. (5) follows from an analytic van der Waals model EOS that accurately captures the experimental EOS data. Simple algebra then yields³⁴

$$\phi(T; A, B, N_s) = 1 + \sqrt{S_0^{\text{expt}}(T)} - \sqrt{S_0^{\text{expt}}(T) + 3\sqrt{S_0^{\text{expt}}(T)}}. \quad (6)$$

Knowledge of $\phi(T)$ then allows $S(k)$ in Eq. (1) to be computed as a function of temperature, which thereby determines the dynamic free energy, from which all dynamical results follow.

Representative calculations of the dynamic barriers (in units of $k_B T$) are shown in Fig. 1(a) for microscopic parameters³⁵ (A , B , N_s , d) relevant to PS. The main frame shows that the local barrier dominates at high temperatures, but grows weakly with cooling. The elastic barrier is essentially negligible at high temperatures because the jump distance and local stiffness (K_0) of the liquid are relatively small, but then increases very rapidly with cooling below a well-defined temperature that signals the crossover to strongly cooperative dynamics.^{34,35} Physically, this increase is due to both a growing jump distance (which sets the amplitude of the strain field outside the cage) and an increase of liquid stiffness. We note that 90% of the elastic barrier is achieved within a distance of roughly 13 particle diameters from the local rearrangement, as shown in the inset to Figure 1, corresponding to ~17 nm for PS.³⁵ It is in this scale-free sense that the elastic barrier is of spatially “long range” origin.

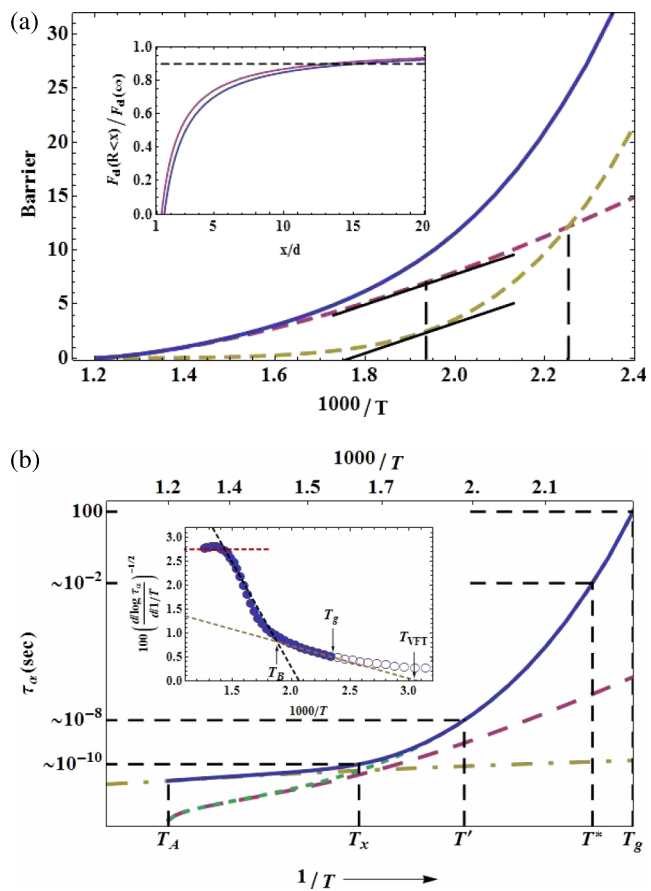


FIG. 1. (a) Dynamic free energy barriers (units of $k_B T$) of bulk polystyrene (PS) liquid versus inverse temperature. Molecular parameters (see text) for PS are³⁵ $A = 0.618$, $B = 1297$ K, $N_s = 38.4$, and $d = 1.2$ nm. Results are shown for the total barrier (solid blue curve), local barrier (red dashed), and elastic barrier (yellow dashed). Solid black lines with a dashed vertical show where the slope of the two barriers is equal, corresponding to the empirical dynamic crossover temperature discussed in the literature. The vertical dashed black line shows where the two barriers are equal, which is much closer to the T_g . Inset: Fraction of the elastic barrier due to integration over the strain field out to a distance R . The blue curve is at the theoretically predicted bulk glass transition temperature of $T_g = 425$ K, and the red curve is at a very high temperature near the onset of activation ($T_A = 795$ K). Note that although the fraction of the total elastic barrier as a function of distance is similar at both temperatures, the absolute magnitude of the barrier is very different. (b) Bulk alpha relaxation time for PS (solid blue) as a function of inverse temperature; the bottom axis defines characteristic temperatures while the top axis indicates the absolute temperature. Results are shown using only the local barrier (red dashed), the elementary short relaxation time τ_s (yellow dashed-dotted), and the activated relaxation time only (green dotted; second term in Eq. (7)). The characteristic temperatures predicted by the theory are: T_A where barrier first emerges (corresponding to an alpha time of 1.5×10^{-11} s at 829 K); T_x where the activated and short time scale contributions to the alpha time are equal in Eq. (7) (9.2×10^{-11} s at 596 K); T' where the inverse temperature derivative of the local and collective elastic barriers are equal (corresponding to an alpha time of 1.15×10^{-8} s at 516 K); T^* where the magnitude of the collective elastic and local cage barriers are equal (corresponding to an alpha time of 0.04 s at 443 K); and T_g where the alpha time equals 100 s at 425 K. Inset—a so-called Stickel derivative plot³⁸ of the alpha time calculation of the main frame showing a high temperature apparent Arrhenius regime, an apparent crossover at T_B (where the alpha time equals 2.4×10^{-9} s at 532 K), T_g , and an extrapolated temperature where the alpha time hypothetically diverges at a temperature $T_{VFT} = 328$ K. The open circles show that the theoretical alpha time never literally diverges.

The mean alpha relaxation time is computed using Kramers theory. Below the onset temperature T_A , and when significant barriers exist, one has³³

$$\frac{\tau_\alpha}{\tau_s} = 1 + \frac{2\pi(k_B T/d^2)}{\sqrt{K_0 K_B}} e^{(F_B+F_{elastic})/k_B T}, \quad (7)$$

where K_B is the absolute value of the barrier curvature. Above and close to the onset temperature (where there is no or small barriers, respectively), the full Kramers expression must be used as discussed previously.³³ The dynamical theory, with the mapping, is *a priori* predictive, and captures well the alpha relaxation time in diverse molecular,^{32,34} and to a lesser extent polymeric,³⁵ van der Waals liquids over 14 decades in time. An example is shown for PS in Fig. 1(b), with characteristic temperatures and times identified as discussed previously.^{34,35} The inset shows the so-called Stickel derivative plot representation.³⁸ An empirical high and low temperature apparent Vogel-Fulcher-Tammann (VFT) behavior is predicted, though ECNLE theory does not have any true divergences above zero Kelvin.

B. Free standing films

A thin film introduces spatial heterogeneity of structure and dynamics that brings many new complications. A vapor interface can, in principle, modify local density, compressibility, and molecular orientation and has a small, but finite, thickness. We believe these are second order effects for free standing films and are ignored in this initial study. We thus assume a sharp interface and a film with density, thermodynamics and intermolecular pair structure identical to that in the bulk. Thus, we emphasize two *generic dynamical* mechanisms of how a free surface modifies the spatially nonlocal activated relaxation event: (i) a “direct surface” effect close to the interface mainly associated with the loss of nearest neighbors and its effect on the local cage barrier and (ii) a longer range “confinement” effect mainly associated with the cutoff of the strain field at the vapor interface which reduces the collective elastic barrier. These two thin film effects are fundamentally coupled in a spatially heterogeneous manner via gradients of *all* physical properties of the dynamic free energy.

Figure 2(a) schematically depicts the physical effects we focus on. The tagged red particle undergoes an activated relaxation event which involves a large amplitude hop to surmount the local cage barrier. As in the bulk, to accommodate this local event in the fluid requires the particles outside the cage region to elastically expand by a small amount in a harmonic manner. Both barriers are reduced when a particle is less than a cage radius from the surface due to softening of the transient localized state associated with fewer neighbors and the cutoff of the strain field at the free surface. This dynamical softening of the film (larger localization length, smaller modulus, and lower barriers) is a continuous function of distance from the surface, as reflected in the color gradient darkening with depth into the film. At distances further from the surface than r_{cage} , the local barrier and other dynamic free energy properties take on their bulk values. However, the elastic barrier is still reduced due to the finite film volume (cut-off effect) and the softer material near the interface. Because of its longer ranged nature, such modified elastic effects can extend deep into the film. These

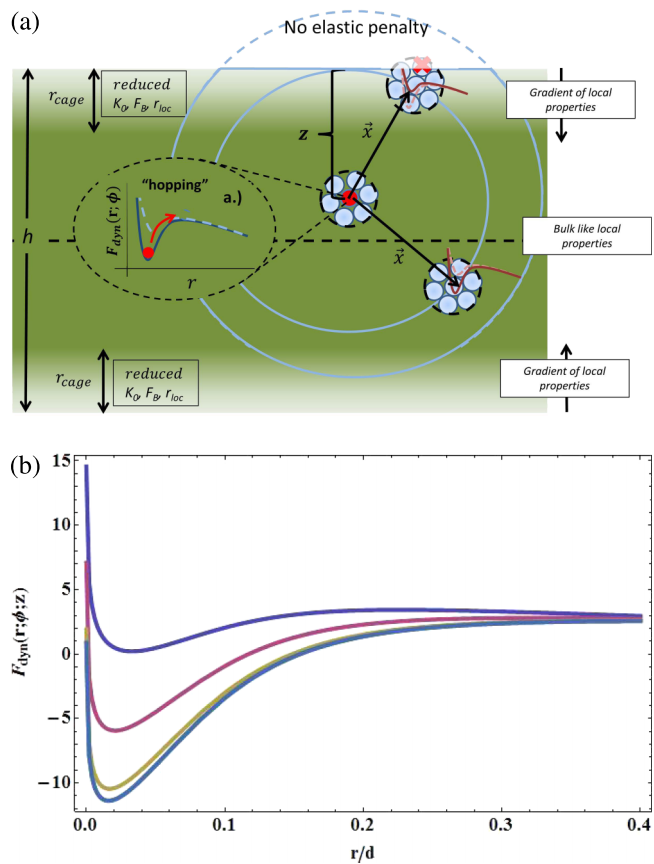


FIG. 2. (a) Schematic illustration of the ideas discussed in the text underlying ECNLE theory for free standing films. (b) Dynamic free energy in units of the thermal energy as a function of reduced particle displacement near the bulk glass transition temperature for a PS film of thickness $h = 15d$ at depths from the surface of $z = 0d$ (blue), $0.5d$ (red), $1d$ (yellow), and the bulk (gray). The dynamic free energy is identical to the bulk analog for any depth $z > r_{cage} \sim 1.33d$.

physical effects are quantified in the ECNLE theory framework as follows.

The local barrier predicted by NLE theory is determined by forces from the nearest neighbor cage particles. Within a distance r_{cage} from a free surface, the number of neighbors, and hence confining forces, is reduced. This is modeled as a reduction of the caging term in the dynamic free energy,³⁶

$$F_{dyn}(r) = F_{id}(r) + \alpha(z)F_{cage}(r). \quad (8)$$

Here, $\alpha(z)$ quantifies the missing nearest neighbors. In the bulk fluid, the number of neighbors is estimated as $N_{nn}^{(bulk)} = \rho \int dv_{cage} = \rho \frac{4\pi}{3} r_{cage}^3$. When a tagged particle is located at a distance $z < r_{cage}$ from the surface, the integration is only over the volume inside the film since the interface is sharp and there are no particles beyond it. Straightforward geometry then results in a reduction of number of nearest neighbors of

$$\begin{aligned} N_{nn} &= \rho \int_0^z dr \int_0^{2\pi} d\phi \int_0^\pi d\theta r^2 \sin \theta \\ &\quad + \int_z^{r_{cage}} dr \int_0^{2\pi} d\phi \int_{\cos^{-1}(z/r)}^\pi d\theta r^2 \sin \theta \\ &= \rho \left[\frac{2\pi}{3} r_{cage}^3 - \frac{\pi}{3} z^3 + \pi z r_{cage}^2 \right]. \end{aligned} \quad (9)$$

The ratio of the prefactor amplitude of the caging part of the dynamic free energy in the film relative to the bulk, $\alpha(z)$, is thus given by

$$\alpha(z) = \frac{N_{nn}}{N_{nn}^{bulk}} = \frac{1}{2} - \frac{1}{4} \left(\frac{z}{r_{cage}} \right)^3 \left[1 - 3 \left(\frac{r_{cage}}{z} \right)^2 \right], \quad (10)$$

$$z \leq r_{cage}$$

$$\alpha(z) = 1, \quad z > r_{cage}.$$

At the surface $\alpha(z \rightarrow 0) \rightarrow 1/2$, recovering the result of Ref. 28, which then smoothly interpolates to the bulk behavior $\alpha(z > r_{cage}) \rightarrow 1$. Figure 2(b) shows a representative calculation of the resulting dynamic free energy at different locations in a PS film based on using Eq. (8) in Eq. (10).

We note that our calculation angularly averages the local forces exerted on a tagged particle by its immediate cage environment corresponding (per Eq. (8)) to retaining a radially symmetric description of the hopping event at a fixed depth (z) in the film. This simplification is adopted for both theoretical consistency and tractability reasons. It also seems to us a reasonable first approximation given the microscopic jump event occurs on a small length scale well below the particle size. Of course, in reality, mobility fluctuations exist in the cage of neighbors that exert forces on a tagged particle which can introduce z -dependent dynamic heterogeneity effects, perhaps of a generalized “dynamic facilitation” nature.³⁰ Moreover, such averaging ignores local one-body density effects such as layering in the direction perpendicular to the film surface. Relaxing these simplifications should be possible and are presently under study.

The presence of $\alpha(z)$ in the dynamic free energy implies that all local properties are modified near the surface of the film. Specifically, the strain or displacement field is taken to be the same functional form as in the bulk,

$$u(\vec{r}; z) = \Delta r_{eff}(z) \left(\frac{r_{cage}}{r} \right)^2 \quad (11)$$

but now the cage expansion length scale, $\Delta r_{eff}(z)$, depends on the position-dependent local dynamic free energy. The strain field is a function of *both* the distance from the cage center and the location of the relaxation event in the film. Equation (11) ignores complicated physical effects that might modify the functional form of the strain field such as distortion of the elastic field at/near an interface and the stiffness gradient, $K_0(z)$, associated with a z -dependent localization length. The true form of the strain field must, in principle, be determined using the appropriate elastic equations taking into account the specific boundary conditions of the film and the modulus gradient near the surface. Addressing this complex issue is an open problem, and will render the theory significantly more computationally intensive. However, we suspect including such effects will result in only quantitative, not qualitative, changes of our results for free standing films.

Incorporating the z -dependent local properties in the expression for the elastic barrier leads to a modification of Eq. (3) given by

$$F_{elastic}(z) = (\rho/2) \int_V d\vec{r} u(\vec{r}; z)^2 K_0(\vec{r}; z), \quad (12)$$

where the integral is over the film volume and K_0 , now position-dependent, controls the localized state vibrational amplitude and material stiffness.^{33–36} Equation (12) leads to a reduction of the elastic barrier via three mechanisms: (i) a position-dependent strain field $u(\vec{r}; z)$, (ii) the position-dependent reduction in local stiffness $K_0(z)$, and (iii) the integration over a finite film volume, i.e., the elastic field cut-off effect. When a relaxation event occurs close to the surface all three effects are important. However, because the integral in Eq. (12) extends over the entire film volume, even events far from the interface (where local properties take on their bulk values) are influenced by a reduced elastic barrier due to the spatial stiffness softening and cut-off effects. Thus, the three contributions are fundamentally and inseparably coupled via the modified local dynamic free energy and the film volume integration in Eq. (12). In contrast to the local barrier, the reduction of the elastic barrier extends well beyond the cage scale, as discussed below.

The mean alpha time associated with activated barrier crossing is still computed using Eq. (7) but all factors now depend on location in the film except for the ultra-short time scale τ_s which is assumed to be unperturbed by thin film confinement.

III. THREE-DIMENSIONAL ALPHA RELAXATION TIME FUNCTION

We now study in detail the alpha relaxation time gradient and its film-averaged analog as a function of the three key variables: depth in the film, z , film thickness, h , and temperature, T . All calculations are done using model parameters for PS melts, but they are representative of a wide class of vdW molecular and polymeric (in the absence of explicit chain connectivity effects) liquids. Based on the Kuhn length^{35,39} as the molecular coarse graining variable, the effective diameter of a PS Kuhn sphere³⁵ is $d \sim 1.3$ nm. The theoretically predicted glass transition temperature in the bulk is $T_g = 425$ K, which is $\sim 15\%$ higher than the experimental value. Spatial gradients of dynamical properties will be shown as a continuous function of location in the film, but one should keep in mind that experiments have a finite resolution, perhaps of order (0.5–1) d .

A. Mobility gradient: Temperature dependence at fixed film thickness

Relaxation time profiles are shown in Figure 3 at fixed film thickness (18 nm) for various temperatures corresponding to a 10 decade variation of the bulk alpha time. Near the bulk T_g , there is a difference of nearly 9 orders of magnitude between dynamics in the film and at the surface due to a reduction of both barriers at the interface relative to their bulk values. Thus, the alpha time is massively faster near the surface, where it varies weakly with temperature. The calculation at 515 K mimics the behavior at the empirically defined dynamic crossover temperature of $T_c \sim 1.2T_g$. In ECNL theory, T_c has a well-defined physical meaning as the characteristic temperature above which the collective elastic barrier aspect

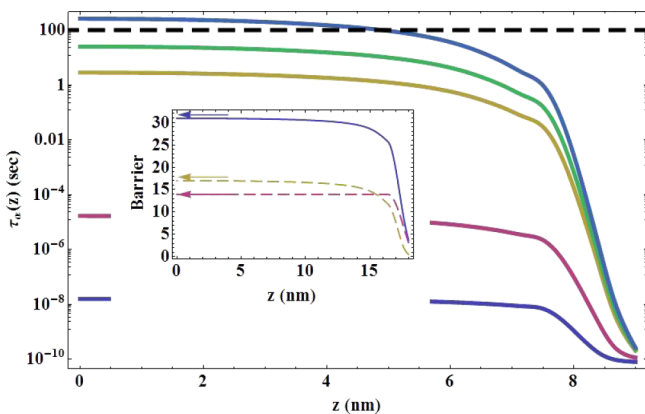


FIG. 3. Alpha relaxation time gradient profile for a PS film of thickness 18 nm. From bottom to top the temperatures are 515 K (blue curve, near bulk $T' \approx T_g$), 470 K (red), 430 K (yellow), 425 K (green, bulk T_g), and 420 K (gray). The dashed horizontal black line at 100 s indicates the criterion used to define a local T_g and mobile layer thickness. Inset—barriers (in units of $k_B T$) as a function of distance from the center of a PS film of thickness 36 nm near the bulk T_g . The solid blue curve is the total barrier, dashed red curve is the local barrier, and the dashed yellow curve is the collective elastic barrier. The arrows of corresponding colors mark the barrier value in the bulk. At 18 nm from the surface, the elastic barrier (and therefore the total barrier) does not quite reach its bulk value.

does not yet play a major role, even for bulk dynamics.^{34,35} This is the regime presumably probed in most simulations, and the long relaxation time tail into the film is largely absent since elastic distortion is very weak, and the gradient covers only $\sim 3\text{-}4$ decades. This modest gradient is mainly associated with the local barrier and loss of near-surface neighbors.

The inset of Figure 3 shows the behavior of the local, elastic, and total barrier heights as a function of distance from the center of the PS film ($z = 0$ here) of thickness 36 nm near the theoretical bulk T_g ; we recall^{34,35} that the bulk barriers at kinetic vitrification are $F_B \approx 14k_B T$ and $F_{\text{elastic}} \approx 18k_B T$. The local barrier is strongly reduced close to the surface (by up to 80% of its bulk value) but quickly recovers its bulk value (marked by an arrow of corresponding color) at a depth equal to the cage radius, r_{cage} . In qualitative contrast, the elastic barrier, while also strongly reduced near the surface, is suppressed far into the film as a consequence of the nonlocal nature of the alpha process in ECNLE theory and its coupling to near-surface cage weakening. This nonlocality implies that for thin enough films (less than $\sim 25\text{-}30$ nm), no true bulk-like region exists.

To further emphasize that the elastic barrier in films is intimately coupled to the local cage scale physics, we considered an “uncoupling approximation” where the z -dependent localization well curvature, $K_0(z)$, and cage expansion length, $\Delta r_{\text{eff}}(z)$, that enter elastic barrier are set by hand to their bulk values everywhere in the film. Thus, reduction of the elastic barrier occurs solely due to the confining geometry. Our numerical calculations based on this gross simplification (not shown) find that ignoring softening of the local barrier and the associated local dynamical properties at the surface incurs large *underestimates* of the reduction of the elastic barrier in thin films (e.g., by a factor of 2), except very deep in the film interior. This further underscores the idea of a fundamental *inseparability* between “local cage” and

“long range elastic” effects in deeply supercooled liquids and films.

B. Layer-resolved temperature dependence of the alpha time and T_g

Figure 4 shows the growth of the alpha time upon cooling a PS film of $h = 18$ nm at various film depths; the solid black curve is the bulk behavior. The temperature dependence near the surface is extremely weak. Because the jump distance is reduced near the surface (cage softening), the cage expansion is significantly reduced, leading to a major reduction in the elastic barrier. The temperature dependence of the relaxation time near the center of the film is very close to that of the bulk.

Because of the highly heterogeneous dynamics perpendicular to the film interface, a film “glass transition temperature” is not uniquely defined. By taking a local alpha time of 100 s as a vitrification criterion, the inset of Fig. 4 shows a local glass transition temperature profile plotted as a function of the normalized depth for film thicknesses of $h = 6, 18$, and 36 nm. Note the large, of order 100 K, suppression of the vitrification temperature at the free surface. One possible theoretically well-defined definition for the glass transition of the entire film is the average of this vitrification temperature profile,

$$\langle T_g \rangle_h \equiv \frac{1}{h} \int_0^h T_g(z) dz. \quad (13)$$

The mean temperature of Eq. (13) is marked with a vertical dashed line in the main figure and is significantly colder than the bulk T_g . We refer to it as the “pseudothermodynamic” glass transition temperature or “average vitrification” temperature.

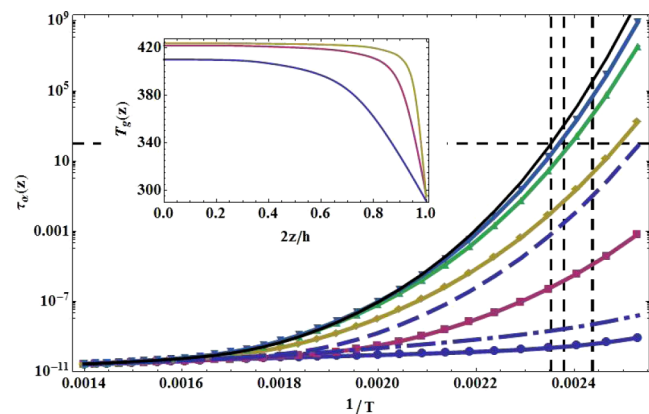


FIG. 4. Alpha relaxation time as a function of inverse temperature for a PS film of thickness 18 nm. The curves are at depths of 0 nm (blue circles), 0.6 nm (red squares), 1.2 nm (yellow diamonds), 3 nm (green triangles), 9 nm (gray triangles—film center), the bulk (solid black). Also shown is the relaxation time and inverse relaxation time averaged over the surface layer to a depth 1.2 nm (dashed blue and dashed-dotted blue curves, respectively). The horizontal dashed line is at 100 s. The intersection of any curve with the latter line defines a depth-dependent local vitrification temperature. The vertical dashed lines represent, from left to right, the bulk glass transition temperature, the temperature at which the average relaxation time in the film is 100 s, and the average local vitrification temperature across the film. Inset—the local vitrification temperature as a function of normalized position in the film for films of thickness 6 nm (blue), 18 nm (red), and 36 nm (yellow).

C. Mobility gradient: Dependence on film thickness and location

Figure 5(a) shows how the alpha relaxation time gradient changes with film thickness at a fixed temperature equal to the bulk T_g . The main frame shows results for films of different thicknesses, where the depth z is normalized by the film thickness. One sees that although on absolute length scales the dynamics are not changing much, the overall *shape* of the normalized profile changes dramatically for thinner films. While the massive speedup of relaxation exactly at the surface is essentially independent of the film thickness, a much larger fraction of the thin film experiences faster dynamics. Indeed, for films thinner than about 30 nm, even the film center does not recover bulk dynamics due to the relatively long ranged elasticity effect. The inset shows the direct effect of film thickness on the relaxation time at a fixed distance from one surface at two different temperatures. In this representation, the effect is only noticeable for quite thin films at depths where the dynamics is modified by the presence of both

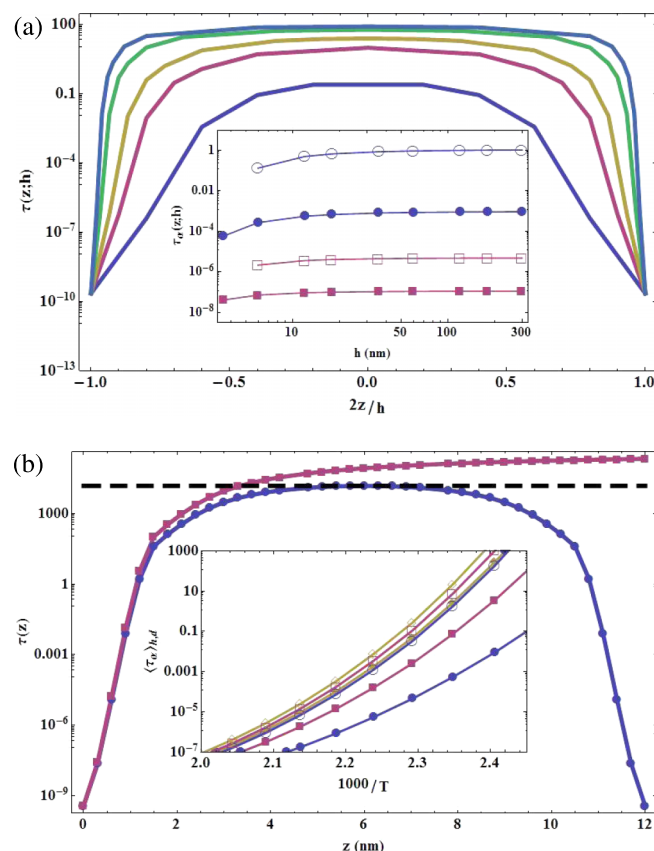


FIG. 5. (a) Relaxation time (s) profile plotted versus the normalized depth in the film at the bulk T_g (425 K) for PS films of thickness (from “inner” to “outer”) 6 nm (blue), 12 nm (red), 18 nm (yellow), 36 nm (green), and 60 nm (gray). Inset—alpha relaxation time as a function of film thickness at depths of 1 nm (solid symbols) and 2 nm (open symbols) from the surface for PS films at 425 K (circles—bulk T_g) and 470 K (squares). (b) Relaxation time (s) profile for a 12 nm thick PS film (blue circles) and the top 12 nm of a 250 nm thick film (red squares) at a fixed temperature of $T_{g,\text{bulk}}=15\text{K}=410\text{ K}$. The horizontal black dashed line is a typical experimental time scale where a thin film dewets (1.5×10^5 s). Inset—the film (closed symbols) and top layer of a bulk sample (open symbols) averaged relaxation time as a function of inverse temperature. Circles have a film/layer thickness of 3.6 nm, squares have a thickness of 6 nm, and diamonds are of 12 nm.

surfaces. Thus, film thickness does not have a large effect on the absolute breadth of the mobility gradient, though in its normalized length scale representation it appears to be large. This behavior can be rationalized based on the “uncoupling approximation” discussed in Sec. III A since the effect of the far surface falls off very quickly compared to the near-surface effect when absolute distances are fixed.

Figure 5(b) shows the isothermal relaxation time gradient in absolute units of depth into the film for a 12 nm thin film and for the top 12 nm of a 250 nm thick film. The latter calculation is relevant to particle embedding measurements^{6,7} that probe the near-surface region of a thick film. The black horizontal line is a crude estimate of the time scale where a thin film would de-wet, 1.5×10^5 s.⁴⁰ At this time scale, we predict that an embedding experiment on a thick film would measure a $\sim 3\text{--}4$ nm thick mobile layer. The inset shows the average relaxation time of a thin film and the top layer of a bulk sample as a function of temperature. The mean alpha time and fragility decrease as the film or layer thickness shrinks.

D. Film-averaged relaxation time and dynamic fragility

Figure 6 shows calculations of the film-averaged relaxation time as a function of temperature for several film thicknesses. The format is an Angell plot, but here the inverse temperature is non-dimensionalized by the *thickness-dependent* “dynamic” T_g defined as

$$\langle \tau_\alpha(T_g) \rangle_h = \frac{1}{h} \int_0^h \tau_\alpha(z; T_g) dz \equiv 100 \text{ s}. \quad (14)$$

The slow parts of the film, being orders of slower magnitude, strongly dominate this average relaxation time. However, the fast regions do impact the temperature dependence in Figure 6. The sharpness of the temperature-dependence of the alpha relaxation can be quantified by the so-called dynamic fragility, $m(h) = [d/d(T_g(h)/T)] \log[\langle \tau_\alpha(T_g) \rangle_h]_{T=T_g(h)}$. Thinner films become more Arrhenius, as quantified by the decreasing

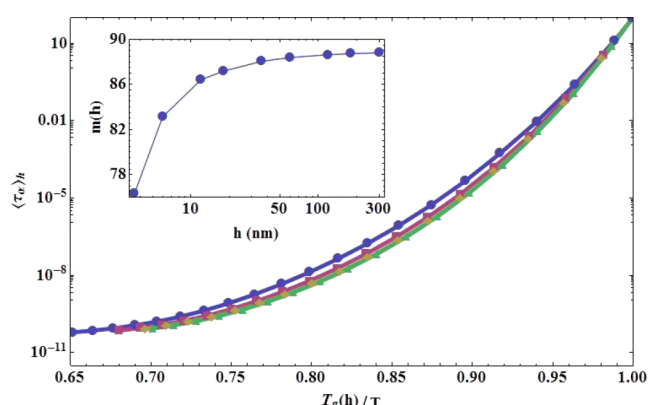


FIG. 6. The film-averaged relaxation time (s) in the Angell format where temperature is non-dimensionalized with the film thickness dependent glass transition temperature for PS films of thickness 3.6 nm (blue circles), 6 nm (red squares), 12 nm (yellow diamonds), and 18 nm (green triangles). Inset—dynamic fragility of the film averaged relaxation time as a function of film thickness.

fragility for thinner films, as shown in the inset to Figure 6. This fragility reduction appears to depend on the “propagation” of faster (and more Arrhenius) dynamics into the film beyond the local cage scale via the long range reduction of the elastic barrier.

IV. NEAR-SURFACE DIFFUSION

Mass transport via center-of-mass diffusion near a film surface is a problem of high scientific and applications interest,^{41–43} including the formation of “ultra-stable” glasses.^{17,18} We briefly study this problem with a minimal model of translational diffusion. Specifically, we define three hopping diffusivities. In the bulk homogeneous material,

$$D_{\text{bulk}} \approx \frac{d^2}{6\tau_{\alpha,\text{bulk}}}. \quad (15)$$

In the heterogeneous thick film, we define a diffusion constant associated with averaging the near-surface layer dynamics to different penetration depths, w . One can perform the average in two ways,

$$D_{\text{surface},B} \approx \frac{d^2}{6}\langle 1/\tau_{\alpha,\text{bulk}} \rangle_w, \quad (16)$$

$$D_{\text{surface},A} \approx \frac{d^2}{6\langle \tau_{\alpha,\text{bulk}} \rangle_w}. \quad (17)$$

It is perhaps *a priori* unclear which of these simple estimates is more realistic for small molecules (e.g., orthoterphenyl (OTP)⁴²). Equation (17) effectively assumes that the relevant total friction constant is its average from the surface to the penetration depth probed. For polymers, it has been suggested that Eq. (17) is more appropriate due to the effect of chain connectivity which decreases the enhancement of surface diffusion relative to the behavior of small molecules.⁴⁴ Experiments on OTP and trisnaphthalene benzene (TNB)^{41–43} also appear to suggest that Eq. (17) is appropriate, where the penetration depth is the molecular size.⁴⁴

Figure 7 shows calculations using molecular parameters relevant to PS for two small penetration depths of $w = 0.5d$

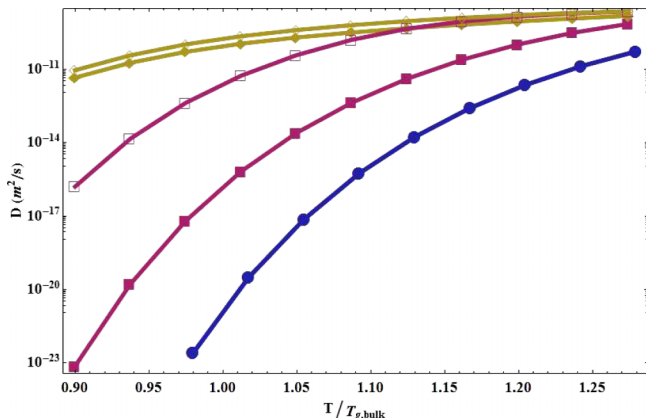


FIG. 7. Hopping diffusion constants (in squared meters per second) defined in the text: bulk liquid (blue circles), surface diffusion constant based on Eq. (17) (red squares) and Eq. (16) (yellow diamonds). Closed (open) symbols average over a surface layer of depth $1d$ ($0.5d$) in a bulk film.

and d. The bulk liquid analog is shown for comparison. All estimates correspond to massively faster surface diffusion compared to the bulk. Based on Eq. (17), transport is 4 or 8 decades faster at the bulk T_g for $w = d$ and $0.5d$, respectively. These values bracket experimental results obtained for aromatic molecular systems which find 6–8 decades of enhancement.^{41–44} If Eq. (16) is employed, the diffusivity is even faster since the more rapidly relaxing regions strongly dominate mass transport. Here, the speed up at T_g is ~ 10 decades, which seems too large compared to recent experiments.^{41–44}

V. DYNAMIC EXPERIMENTS

Although the dynamics of spatially heterogeneous thin films is fundamentally characterized in terms of the 3-dimensional alpha relaxation time surface, $\tau_\alpha(T, h, z)$, experiments cannot directly probe it. Thus, in this section we apply the theory to predict the implications of the mobility profile for measured quantities in the time and frequency domains.

A. Time domain correlations and extraction of time scales

One of the most direct probes of local dynamics is the dye rotation experiments of Paeng and Ediger.⁵ By measuring the decay of the fluorescence intensity due to dye reorientation in a polymer matrix, they extract a dynamical measure of the local alpha relaxation process. Assuming that the fluorescence intensity of a dye molecule decays exponentially according to the local relaxation time, the average fluorescence intensity of the film is related to the correlation function as

$$C(t) = \langle e^{-t/\tau(z;T;h)} \rangle_h, \quad (18)$$

where the average is performed over the film thickness, h .

Calculations of $C(t)$ are shown in Figure 8(a) for several temperatures and $h = 30$ nm. As done in the experimental data analysis,⁵ we fit our calculations to a KWW stretched exponential function over a time window of about 6 orders of magnitude. In accord with the experiment, we find that at lower temperatures a double KWW function of the form

$$C(t) = a_1 e^{-(t/\tau_{\text{fast}})^{\beta_1}} + a_2 e^{-(t/\tau_{\text{slow}})^{\beta_2}} \quad (19)$$

is needed to satisfactorily fit the theoretical data, while at higher temperatures a single KWW function is sufficient. The fast and slow times extracted from the best fits are shown in the inset to Fig. 8(a). In accord with what has been indirectly inferred from the experiment,⁵ the smaller relaxation time is due to the fast dynamics near the film surface, while the slow process is due to the bulk-like process in the film interior. However, it should be noted that this discrete two-time scale picture arises from the interpretation of a continuous mobility gradient within the empirical framework of an effective 2-layer model.

Examining the inset of Fig. 8(a) in detail, one sees that the short time side of the two KWW fit deviates from the linear fit shown at that temperature. This reflects subtleties of

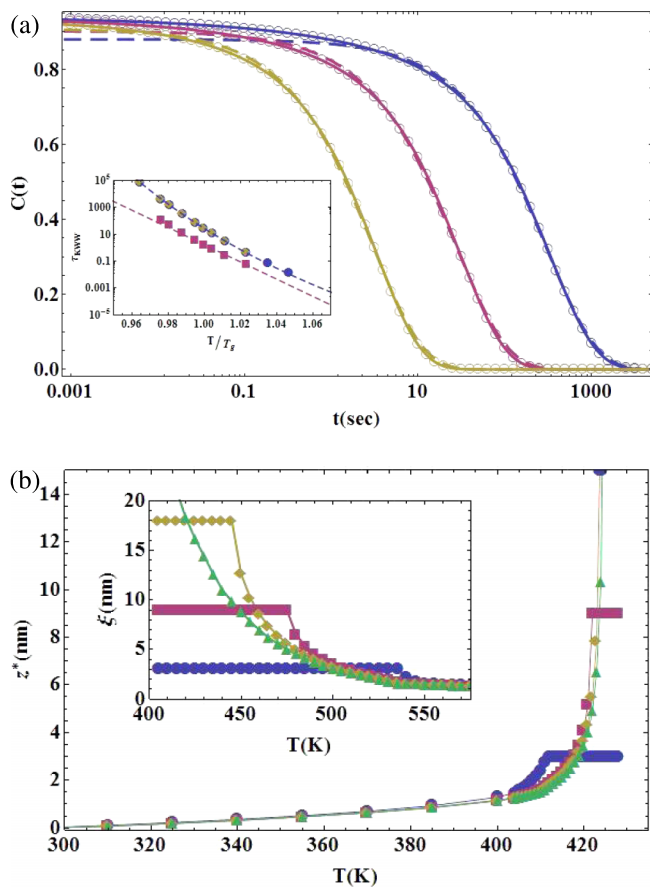


FIG. 8. (a) Film-averaged time dependent correlation function of Eq. (18) as a function of time (s) for a PS film of thickness 30 nm at temperatures of 420 K (blue circles), 425 K (red circles—bulk T_g), and 430 K (yellow circles). The solid curves are fits to a double KWW form of Eq. (19) and the dashed curves are fits to a single KWW form. Inset—extracted KWW relaxation times. Blue circles are for the single KWW fit, red squares are the fast time, and yellow diamonds are the slow time for the double KWW fit. A VFT fit is shown for the long times, while the fast time is a linear fit. Extrapolation of the fitted curves does not intersect at high temperatures. (b) Thickness of a mobile layer at the surface of a PS film defined by Ref. 5 where the relaxation time is faster than 100 s. Inset—length scale defined²⁵ as the fraction of the film faster than 80% of the bulk relaxation time as a function of temperature. Results are shown in both panels for films of thickness 6 nm (blue circles), 12 nm (red squares), 18 nm (yellow diamonds), and 36 nm (green triangles).

both the fitting procedure and the existence of a continuous gradient of dynamics. Specifically, the longer relaxation times have mostly moved outside the fitting window, and the short time process is influenced by both the fast surface region dynamics and some faster portions of the inner region. The difference between the fast and slow relaxation times grows with cooling from about a factor of 10 to a factor of 40 at low temperatures. Empirically extrapolating both the slow and fast times *linearly* to high temperatures does lead to an intersection at 445 K = $T_{g,\text{bulk}} + 20$ K (not shown). However, using a VFT form to fit the slow relaxation time data results in the disappearance of this apparent intersection.

We find that the amplitudes and exponents of the KWW fits in Fig. 8(a) are essentially linear functions of temperature. The single KWW amplitude is nearly constant at ~0.89, with a KWW exponent that grows with heating linearly from 0.72 to 0.85 over the temperature range studied. The two KWW function fit has an essentially constant short time

amplitude of 0.15, except at 410 K where it increases to 0.2. The long time amplitude is nearly constant at ~0.75–0.78. The short time process stretching exponent increases linearly and strongly with temperature from 0.23 at 410 K to 0.47 at the highest temperature studied of 435 K. Thus, for the near-surface region, thin film confinement greatly increases dynamic heterogeneity as encoded in the breadth of the relaxation time distribution. The long time (film interior) exponent increases linearly from 0.78 to 0.89 over the same temperature range.

Although the qualitative picture that emerges from our calculations is broadly consistent with the experiment and the coarse interpretative idea of a “two-layer model,”^{2,5,22} direct quantitative comparison is difficult for several reasons. First, experiment measures the rotational relaxation of a probe dye molecule as a proxy for the relaxation of the film.⁵ Although they may correlate well, the dye will perturb the packing in the surrounding liquid and this may subtly affect the measured dynamics. Such local packing effects (including dye alignment) could be particularly important near an interface. Experiments are also, of practical necessity, limited to a time window of about 6 decades. Although the theory predicts a nearly 11 order of magnitude range of relaxation times in the film at the relevant temperatures, we have performed our fits over a 6 order of magnitude window in time in an attempt to mimic this experimental reality. Changing the width or location (relative to temperature) of the fitting window can lead to quantitatively (but not qualitatively) different results.

Of course, our simple model ignores effects present in real materials. The treatment of the microscopic density profile as a step function may be relevant to describing the fast Arrhenius process seen in experiments. Recent work^{5,45} and earlier embedding experiments^{6,7} measure (indirectly) the film-averaged relaxation time for film of various thicknesses. Over the limited experimentally accessible relaxation time window, extrapolation of the data for thin *polymer* films leads to an apparent intersection with the bulk process, typically a bit above the bulk T_g .^{40,45,46} In contrast, our theoretical calculations when accurately extrapolated (see inset of Fig. 8(a)) appear not to show such an intersection. This might be the “correct” answer since no intersection is observed for molecular liquids (e.g., TNB⁴²) and our model treats polymers as disconnected Kuhn segments per a molecular system. The qualitative agreement of the present theory with small molecule experiments suggests the physical origin of the extrapolated intersection feature above the bulk T_g may be a polymeric, not generic, effect in thin films. Also, such an intersection is not observed in simulations^{23–26} performed in the precursor dynamical regime where the elastic barrier is small or absent. Thus, we speculate that the intersection feature arises from a coupling of the elastic barrier reduction effect and polymer chain connectivity constraints, possibly via stresses propagated along the chain backbone.

B. Extraction of a mobile layer thickness and an alternative length scale

Motivated by the experimental analyses of Paeng and Ediger,⁵ the main frame of Figure 8(b) shows calculations of

a mobile liquid-like layer thickness, z^* , defined as the part of the film that relaxes faster than 100 s. We find, for example, $z^* \sim 2\text{-}3 \text{ nm}$ at 5 K below the bulk T_g , consistent with the experiment.⁵ Calculations as a function of temperature for different film thicknesses essentially overlap, as observed,⁵ except right at T_g where by definition $z^* \rightarrow h$. Moreover, if the length scale resolution is of the order of a molecular diameter d , we predict a *measureable* mobile layer is undetectable 30–40 K below the bulk T_g , which is consistent with the observations of Ref. 5. On the other hand, some other types of measurements with different resolution^{6,12} report mobile layers down to 50–80 K below T_g , which is not inconsistent with our results. We believe that the range of various reported temperatures where the mobile layer disappears is due to different experimental probes effectively averaging the local dynamics on distinct length scales. A larger averaging length scale leads to somewhat slower apparent dynamics, and the disappearance of the mobile layer at higher temperatures. Theoretically, we can resolve a mobile “layer” of any thickness, for example, we find that the film retains some mobility down to temperatures more than 100 K below the bulk T_g if one assumes a tiny layer thickness of $\sim 0.1d$.

Experiments that report the apparent presence of a mobile surface layer region that shrinks with cooling seem to suggest a trend that contradicts the seductive paradigm that the bulk glass transition is controlled by an entropy crisis via a CRR of size that grows with cooling.^{27,29} If the speed up in dynamics arises due to cutting off of this CRR length scale, then the spatial range of enhanced mobility might be expected to *increase* with cooling, in contradiction to the experiment. Recently, this apparent contradiction has been put forward as something of a puzzle.² But returning to our microscopic mobility profile (e.g., Fig. 3), a natural (and perhaps obvious) understanding of the shrinking mobile layer is evident. We define a molecule or Kuhn segment as “mobile” if it relaxes faster than some experimental time scale, taken here to be 100 s. As the film is cooled, the thickness of this mobile layer, z^* , changes. The resulting length scale is plotted in Figure 8(b). Consistent with the experimental results and analysis, we find that the mobile layer thickness shrinks with cooling and is largely independent of the film thickness, except for very thin films less than 10 nm thick (thinner than those probed in the experiment). For these thin films, the dynamics near the surface are also appreciably affected by the presence of the opposite surface, leading to a slightly larger mobile layer. At very high temperatures, the mobile layer reaches a maximum at half the film thickness, and it grows smoothly to scales much larger than the cage radius which is reflective of the long-range nature of the elastic barrier and its contribution to the faster dynamics.

Recent simulation studies of Simmons and co-workers²⁵ have explored an alternative definition of a mobile layer length scale, denoted ξ . Rather than comparing the mobility based on a fixed experimental time, their definition compares the mobility profile at a given temperature to the bulk relaxation time at the same temperature. Regions where the relaxation time of the film is faster than the bulk liquid relaxation time *at the same temperature* are defined to be mobile. This definition is a mobility criterion that is *not* isothermal, but rather changes

with temperature. Adopting it leads to a length scale that we predict does grow with cooling (as found in the simulations,²⁵ and also measurements on thin supported polystyrene films⁴⁷), and which is more sensitive to the thickness of the film, as shown in the inset to Figure 8(b). The different temperature dependences of ξ for films of different thicknesses arise from the combined effects of a simultaneously changing microscopic mobility profile shape (which depends on the film thickness) and mobility criterion with temperature.

C. Frequency domain analysis

A common experimental technique for probing thin film dynamics is frequency domain dielectric spectroscopy.^{2,19} To make qualitative contact with these experiments, we calculate the film-averaged loss function which is simply the appropriate Fourier transform of Eq. (18),

$$C''(\omega) = \omega \int_0^\infty dt \cos(\omega t) C(t) = \left\langle \frac{\omega \tau(z)}{1 + (\omega \tau(z))^2} \right\rangle_h. \quad (20)$$

The form of the z -dependent relaxation time used in this average is exactly as that shown in Figures 5(a) and 5(b). The main frame of Figure 9 shows results as a function of temperature at a fixed frequency of 0.01 Hz for various film thicknesses; very similar results are found at 1 and 100 Hz (not shown). At thicknesses larger than $h \sim 50 \text{ nm}$, the dynamics become invariant to film thickness. A large change in the loss function is only readily apparent for the thinnest films with $h < 18 \text{ nm}$. Below this thickness, the peak temperature shifts to lower values indicating a dynamical speed up due to mobile surface layers. The shape of the function also broadens, seemingly suggesting increased dynamic heterogeneity in the film. However, from our theoretical knowledge of the real space mobility profile, we know that the absolute difference

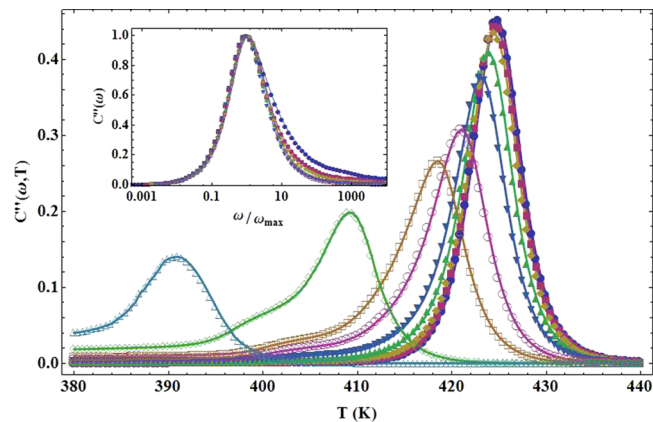


FIG. 9. Model dielectric loss function of Eq. (20) at a fixed frequency $\omega = 0.01 \text{ Hz}$ as a function of temperature for PS film thicknesses (from left to right) 3.6 nm, 6 nm, 12 nm, 18 nm, 36 nm, 60 nm, 120 nm, 180 nm, and 300 nm. A dynamic T_g can be extracted from the peak of each curve. Thicknesses larger than 60 nm essentially overlap. Inset—dielectric loss function at the bulk $T_g = 425 \text{ K}$ as a function of frequency normalized by the peak value for PS film thicknesses 18 nm (blue circles), 36 nm (red squares), 60 nm (yellow diamonds), 120 nm (green triangles), 180 nm (gray triangles), and 300 nm (open circles). The thinnest films show an excess wing of intensity.

between the surface and center relaxation times *decreases* for thinner films. The relaxation time at the film center never reaches that of the bulk for thin enough films, and thus is more Arrhenius than the bulk, so the temperature range of the dynamic response is larger than in thicker films.

Qualitatively, it seems reasonable to infer that the dynamical connection between our results in Figures 5 and 9 is that the position of the main dielectric peak is a rough measure of the relaxation time in the film interior, while the higher frequency/lower temperature shoulder reflects the alpha time near the film surface. The latter depends on the overall film thickness.

As will become clear in Sec. VI, the temperature shifts in Fig. 9 are very similar to our predictions for the depression of an apparent T_g calculated using the *most dynamic* averaging procedure of Eq. (14). However, the shifts are significantly smaller than those obtained based on $\langle T_g(z) \rangle_h$ of Eq. (13), and the pseudo-thermodynamic ellipsometry calculations discussed in Sec. VI. This difference seems germane to the findings of some workers¹⁹ of much smaller dynamical perturbations in thin films based on dielectric measurements compared to pseudo-thermodynamic experiments.

The inset to Figure 9 shows the normalized loss function as a function of frequency at a fixed temperature. As the film thins, the peak frequency increases by a modest factor of $\sim 3\text{-}4$ (not shown). This is a far less dramatic effect than the 1-2 orders of magnitude difference between the fast and slow process deduced from the time domain analysis of $C(t)$ in Section V A. Overall, a quite a good collapse is found, but systematic broadening (excess wing) on the high frequency side of the peak emerges below $h \sim 18$ nm, and grows in amplitude as films become even thinner. This is a signature of the presence of fast (mobile layer) and slow processes in the time domain. It arises due to the increased importance of the more mobile region of the film in determining the average behavior, not an absolute wider range of relaxation times in thinner films. In fact, in thicker films, the highly mobile region is a small portion of the sample that is swamped in the averaging and not visible in the final result.

VI. T_g SHIFTS: PSEUDO-THERMODYNAMIC VERSUS DYNAMIC

Ellipsometry measurements detect changes of the thermal expansion coefficient of a material and are widely used to study glassy thin films.^{1,2,8-10} We employ our calculated mobile layer thickness from Section V B, z^* , and the predicted continuous mobility gradient to construct an effective two-layer model.^{2,22} The mobile layer is assigned a thermal expansivity, $\alpha_l = 0.0004 \text{ K}^{-1}$ and the immobile or vitrified layer a thermal expansivity $\alpha_g = 0.0001 \text{ K}^{-1}$, values relevant to PS. The effective film expansivity is then taken as

$$\alpha_{eff}(T) = \alpha_g z^*(T) + \alpha_l [1 - z^*(T)]. \quad (21)$$

Let h_0 be the film thickness at low temperature T_0 . The film thickness as a function of temperature then becomes

$$h(T) = h_0 \left(1 + \int_{T_0}^T dT' \alpha_{eff}(T') \right) \quad (22)$$

which varies with temperature only via the thickness of the mobile layer.

Calculations based on this model are shown in Figure 10. As an example, for a 6 nm film we indicate how a glass transition is extracted from the “numerical data.” The solid lines represent the extrapolation of the high temperature (“liquid”) and low temperature (“glassy”) regimes. The intersection defines a glass transition temperature, as done in the experiment. The results are shown in Figure 11 as solid blue circles. As observed experimentally,¹⁻³ the breadth of the transition appears to decrease with increasing film thickness. For the 6 nm film, the glass transition temperature decreases by ~ 30 K, an amount comparable to experiments.¹⁻³

For the thinner films, one can perhaps empirically identify a third, quasi-linear regime shown as a dashed line in Figure 10. This allows for the extraction of two apparent glass transition temperatures, as recently reported by Pye and Roth.¹⁰ The upper and lower T_g ’s are shown in the inset of Fig. 11 and are associated with (though not identical to) the initial (final) vitrification of the film center (surface). As the film thickens, the contrast between the two lines that define the lower T_g diminishes and eventually becomes undetectable beyond $h \sim 30\text{-}50$ nm, while the contrast of the upper transition appears to increase. For a sufficiently thick film only a single transition is apparent, which coincides with the upper T_g . This pattern of a higher contrast (and broader) upper transition and low contrast (but narrower) lower transition is reminiscent of experiments on high molecular weight polymer films.^{3,8-10} We find the extracted lower apparent T_g varies linearly with the film thickness, and the upper (and the single) T_g can be fit to the widely employed empirical form⁴⁸

$$T_g(h) = T_{g,bulk} \left(1 - \left(\frac{a}{h} \right)^\delta \right). \quad (23)$$

Fitting our single T_g calculations to Eq. (23) yields $a = 0.46$ and $\delta = 0.94$, while fitting the upper T_g yields $a = 0.41$ and $\delta = 1.06$. Extrapolating the linear fit to the lower T_g data leads to an intersection with the bulk T_g at $h \sim 100$

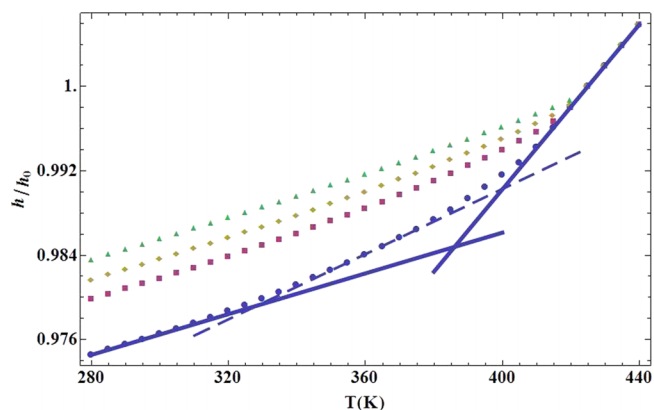


FIG. 10. Model ellipsometry calculation. The total film thickness is plotted as a function of temperature using the effective two-layer model for the thermal expansivity described in the text. Initial thicknesses are 6 nm (blue circles), 12 nm (red squares), 18 nm (yellow diamonds), and 36 nm (green triangles). The solid lines illustrate how T_g can be extracted via fitting to the high and low temperature behavior. For the thinnest films, it is possible to fit the middle region and extract two apparent glass transition temperatures.

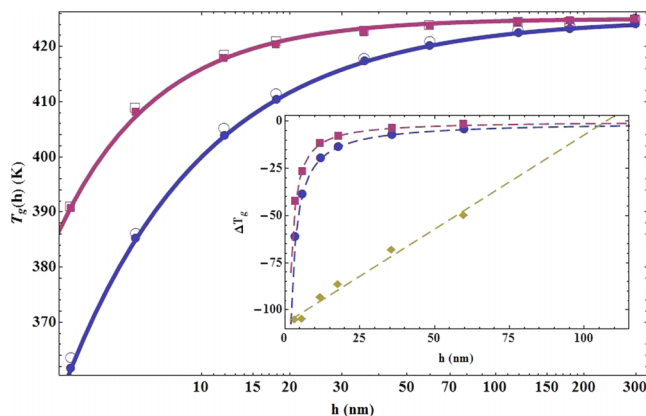


FIG. 11. The glass transition temperature of a PS film as a function of film thickness using various methods of obtaining $T_g(h)$. Blue circles are the average vitrification temperature across the film, $\langle T_g(z) \rangle_h$. The red squares are the temperature at which the average relaxation time of the film is 100 s, $\langle \tau_\alpha(z) \rangle_h = 100$ (s). The open circles are extracted from the ellipsometric calculation of the film expansivity (from Fig. 10) and the open squares are extracted from the peak of the dielectric calculation at $\omega = 0.01$ Hz (Fig. 8(b)). The agreement between the pairs of calculations discussed in the text justifies our use of the verbiage “pseudo-thermodynamic” T_g and “dynamic” T_g . The solid curves are fits to the solid points of corresponding color using Eq. (23); the blue curve has $a = 0.44$ and $\delta = 0.91$, and the red curve has $a = 0.51$ and $\delta = 1.29$. Note that δ is close to unity in both cases, and the points can be adequately fitted by setting $\delta = 1$ and adjusting only one parameter (Eq. (24)). Inset—film T_g shift extracted via fitting of the ellipsometry calculations per Fig. 10. The blue circles are fits that extract a single T_g , red squares are the “upper” T_g of the two T_g fit, and the yellow diamonds are the “lower” T_g . Dashed blue and red curves are fits to Eq. (23) where the blue curve (single T_g) has $a = 0.46$ and $\delta = 0.94$ and the red curve (“upper” T_g) has $a = 0.41$ and $\delta = 1.06$. The yellow line is a linear fit $T_g(h) - T_{g,bulk} = cT - b$, with $c = 1$ and $b = 1.07$.

nm. These numbers are qualitatively (though not necessarily quantitatively) consistent with the experiment.^{1–3,6–10}

Several cautionary comments are in order concerning the fitting of ellipsometric data and our analysis. First, Eq. (23) is not a unique representation of our calculations. We have previously showed³⁶ that the thickness dependences of our theoretically computed glass transition temperatures can be well fitted by the alternative form employed in various experimental and simulation studies,²³

$$T_g(h) = T_{g,bulk}(1 + \xi/h)^{-1}, \quad \xi < d. \quad (24)$$

At present, we have no rigorous theoretical basis for Eqs. (23) and (24), and they are employed here simply as useful empirical expressions to analytically express our theoretical data. Second, when data quality allows, experimentalists often plot the *slope* of the thickness data as a way to more accurately obtain a glass transition temperature. If such a plotting analysis is applied to our calculations, then from the definition of α_{eff} and Eq. (21), our plot will have a shape identical to $z^*(T)$ curves in Figure 8(b). Thus, the two “transitions” we extract are only *apparent*, since a true transition would appear as another horizontal line which then changes to a horizontal line at a different level. We believe the best interpretation of our results is that the underlying physics is simply that a broad and continuous range of “local vitrification” temperatures exist throughout the film (inset to Fig. 4), which are being experimentally detected in an effective sense as two apparent glass transitions. The predicted transition is exceedingly broad

and spans up to 120 K, as shown in the inset to Figure 4. Experiments which do not cover a large enough range of temperatures will detect only a single transition. Third, while the upper T_g appears to be experimentally insensitive to the polymer chain length, the experimental lower T_g depends on the molecular weight and is clearly seen only for long chains.^{6–10} When the linear fits of the data from samples of different molecular weights are extrapolated to thicker films, there is an intersection at 80–100 nm well above the bulk T_g . At present, our theory treats, even in the bulk, polymer liquids as disconnected segments of Kuhn segments.³⁵ As such, it is blind to longer range chain connectivity effects which appear to be important in reality for some questions and effects. The Kuhn model and packing structure presently employed also ignores effects such as molecular layering and orientation at and near the surface. Thus, even if we take seriously the physical interpretation of the theoretically lower T_g as a representation of the final vitrification of the film surface, it seems that the theory at best crudely captures a generic possible mechanism for the apparent lower transition.

As we previously mentioned, the calculation of T_g for a thin film is not a well-defined or unique task. However, the ability of the theory to calculate a relaxation time profile does allow a new insight. Figure 11 compares the theoretically defined “pseudo-thermodynamic” T_g with the glass transition extracted from fitting our ellipsometry model calculations (with a single T_g). We find almost perfect agreement between these two different calculations. This suggests that pseudo-thermodynamic techniques such as ellipsometry perform a specific average of the microscopic dynamics in the film — namely, they are sensitive to the mean “vitrification” temperature of the film. Figure 11 also shows that the theoretically well-defined “dynamic” T_g of Eq. (14) is in good agreement with the glass transition temperatures extracted from our model dielectric loss calculations. Thus, we conclude that within the context of our model and theory, dynamical experiments, such as dielectric measurements, perform an average of the relaxation time across the film. Different experimental techniques effectively perform different averages of the *same*, highly heterogeneous, mobility profile in the film, and thus report different apparent dynamics. It is hoped that our new ability to *a priori* predict the shape of the microscopic mobility profile will help reconcile some seemingly contradictory experimental results and spur new experiments that can provide further insight.

As a caveat to our suggestion that dielectric measurements probe a film-averaged relaxation time, we emphasize that this is only an operational statement in the sense that a film “ T_g ” can be defined and computed from our model dielectric relaxation spectrum as described above. We are not making any broader statements about the connection of our results to the laboratory dielectric spectrum or distribution of logarithmic relaxation times.

VII. CONCLUDING REMARKS

We have constructed a quantitative, force level theory for how confinement in free-standing thin films introduces a

mobility gradient as encoded in the 3-dimensional function $\tau_\alpha(T, z, h)$. A crucial idea is that the rich behavior predicted reflects the modification of *both* near-surface barriers due to a reduced number of nearest neighbors in the local cage and the spatial cutoff and dynamical softening near the vapor interface of the longer range collective elasticity cost for large amplitude hopping. These two effects are fundamentally coupled. Diverse consequences appear consistent with observations of dynamical and pseudo-thermodynamic experiments.

Much work remains to be done at the level of fundamental statistical mechanics. The present theory treats the film to be of fixed volume with an idealized surface. Incorporating effects such as surface fluctuations into the theory may require additional thermodynamic variables beyond the dimensionless compressibility, such as surface tension. Our simplification that only the strain field amplitude, and not its functional form nor symmetry, is modified under planar confinement requires future development. This is a difficult problem even in continuum elasticity due not only to the symmetry-breaking boundary condition issue but also the fact that the local material stiffness (encoded in the localization length of the dynamic free energy) varies strongly and continuously across the film. However, we suspect that the key leading order physical idea will remain the cutoff of the deformation field at a vapor interface. The theory at present computes only the mean alpha time as a function of spatial location in the film. In this sense it captures spatial dynamic heterogeneity, but intrinsic heterogeneous^{6,49} and facilitated³⁰ dynamics present even in the globally homogeneous bulk remain to be explicitly taken into account. We have also only addressed relaxation dynamics. Predicting the high frequency elastic properties of the film, both in an averaged and spatially resolved gradient manner, remains an open problem that will be addressed in a forthcoming article.⁵⁰ To treat films on solid supports of variable chemistry and elasticity, or the analogous capped films, is even more challenging. Both the cage scale activation event and the corresponding elastic deformation field will require re-thinking to include a surface hard boundary condition of variable stiffness and wettability in the basic theoretical approach.

Concerning the model employed here for free standing films, several directions are plausible to immediately pursue. The quantitative influence of chemistry on mobility gradients and T_g shifts should be possible to address based on our mapping ideas which have been shown to have some chemical predictability in the bulk.^{34,35} The nonzero, but narrow, width of the liquid vapor interface can be treated by allowing the film density to vary continuously from zero to its bulk value near the surface. Results for these two aspects will be reported elsewhere.⁵⁰ Our approach should be relatively straightforward to generalize to other confinement geometries, e.g., spherical droplets.⁵¹ As the confining geometry changes, the importance of the cutoff of the strain field at the vapor interface compared to the more local loss of cage neighbors will change. For long polymers, connectivity beyond the Kuhn scale is critical to understand chain dynamics and center-of-mass diffusion. This is a challenging problem since different Kuhn segments of a chain will be located at different places in the film and experience variable friction constants,

leading to the possible dynamic pinning of chains near the interface.^{40,44}

Finally, we mention fascinating creep experiments by McKenna and co-workers on free standing thin films which find that the glassy mechanical modes of films *stiffen*, not soften, as they thin.⁵² It is not easy to reconcile this observation with probe rotation and other local relaxation data that strongly suggest the presence of a mobile layer at the surface. We believe a key practical point is that the creep experiments are not done isothermally. That is, as the film thins, the measurement is done (for practical reasons) at a temperature roughly a fixed absolute distance from the *film* glass transition temperature, $T_g(h)$, not a fixed absolute temperature. Since T_g decreases as the film thins, the experiments are done on colder samples for thinner films. Thus, subtle competing effects are at play which might result in qualitative changes of the functional form of the mobility gradient when films at different temperatures and thicknesses are compared. This problem can be studied with the present theory in a systematic manner, and results will be reported in our next publication.⁵⁰

ACKNOWLEDGMENTS

This work was supported by the U.S. Department of Energy, Basic Energy Sciences, Materials Science Division via Oak Ridge National Laboratory. Stimulating and informative discussions with Mark Ediger, Zahra Fakhraai, Greg McKenna, Justin Pye, Rob Riggelman, Connie Roth, Sindee Simon, David Simmons, Alexei Sokolov, Michael Vogel, and Lian Yu are gratefully acknowledged.

- ¹M. Alcoutlabi and G. B. McKenna, *J. Phys.: Condens. Matter* **17**, R461 (2005).
- ²M. D. Ediger and J. A. Forrest, *Macromolecules* **47**, 471 (2014).
- ³J. A. Forrest and K. Dalnoki-Veress, *Adv. Colloid Interface Sci.* **94**, 167 (2001).
- ⁴R. Richert, *Annu. Rev. Phys. Chem.* **62**, 65 (2011).
- ⁵K. Paeng, S. F. Swallen, and M. D. Ediger, *J. Am. Chem. Soc.* **133**, 8444 (2011); K. Paeng and M. D. Ediger, *Macromolecules* **44**, 7034 (2011); K. Paeng, R. Richert, and M. D. Ediger, *Soft Matter* **8**, 819 (2012).
- ⁶D. Qi, M. Ilton, and J. Forrest, *Eur. Phys. J. E* **34**, 1 (2011).
- ⁷Z. Fakhraai and J. A. Forrest, *Science* **319**, 600 (2008).
- ⁸J. A. Forrest, K. Dalnoki-Veress, J. R. Stevens, and J. R. Dutcher, *Phys. Rev. Lett.* **77**, 2002 (1996).
- ⁹J. Mattsson, J. A. Forrest, and L. Börjesson, *Phys. Rev. E* **62**, 5187 (2000).
- ¹⁰J. E. Pye and C. B. Roth, *Phys. Rev. Lett.* **107**, 235701 (2011).
- ¹¹Z. Fakhraai and J. A. Forrest, *Phys. Rev. Lett.* **95**, 025701 (2005); D. Qi, Z. Fakhraai, and J. A. Forrest, *ibid.* **101**, 096101 (2008).
- ¹²Y. Chai, T. Salez, J. D. McGraw, M. Benzaquen, and K. Dalnoki-Veress, *Science* **343**, 994 (2014).
- ¹³M. D. Ediger and P. Harrowell, *J. Chem. Phys.* **137**, 080901 (2012); L. Berthier and G. Biroli, *Rev. Mod. Phys.* **83**, 587 (2011).
- ¹⁴J. A. Forrest, *J. Chem. Phys.* **139**, 084702 (2013).
- ¹⁵C. J. Ellison, M. K. Mindra, and J. M. Torkelson, *Macromolecules* **38**, 1767 (2005).
- ¹⁶A. Bansal, H. C. Yang, C. Z. Li, K. W. Cho, B. C. Benicewicz, S. K. Kumar, and L. S. Schadler, *Nat. Mater.* **4**, 693 (2005); J. Berriot, H. Montes, F. Lequeux, D. Long, and P. Sotta, *Macromolecules* **35**, 9756 (2002); J. Moll and S. K. Kumar, *ibid.* **45**, 1131 (2012); P. Rittigstein, R. D. Preistley, L. J. Broadbelt, and J. M. Torkelson, *Nat. Mater.* **6**, 278 (2007).
- ¹⁷S. F. Swallen, K. L. Kearns, M. K. Mapes, Y. S. Kim, R. J. McMahon, M. D. Ediger, T. Wu, L. Yu, and S. Satija, *Science* **315**, 353 (2007); K. L. Kearns, S. F. Swallen, M. D. Ediger, T. Wu, Y. Sun, and L. Yu, *J. Phys. Chem. B* **112**, 4934 (2008).
- ¹⁸K. J. Dawson, K. L. Kearns, L. Yu, W. Steffan, and M. D. Ediger, *Proc. Natl. Acad. Sci. U. S. A.* **106**, 15165 (2009).

- ¹⁹M. Tress, M. Erber, E. U. Mapese, H. Huth, J. Mueller, A. Serghei, C. Schick, K. J. Eichorn, B. Volt, and F. Kremer, *Macromolecules* **43**, 9937 (2010); V. M. Boucher, D. Cangialosi, H. Yin, A. Schönhals, A. Alegria, and J. Colmenero, *Soft Matter* **8**, 5119 (2012); K. Fukao and Y. Miyamoto, *Phys. Rev. E* **64**, 011803 (2001); S. Kawana and R. A. L. Jones, *ibid.* **63**, 021501 (2001).
- ²⁰P. G. de Gennes, *Eur. Phys. J. E* **2**, 201 (2000).
- ²¹C. J. Ellison and J. M. Torkelson, *Nat. Mater.* **2**, 695 (2003).
- ²²J. A. Forrest and K. Dalnoki-Veress, *ACS Macro Lett.* **3**, 310 (2014).
- ²³J. Baschnagel and F. Varnik, *J. Phys.: Condens. Matter* **17**, R851 (2005); P. Scheidler, W. Kob, and K. Binder, *J. Phys. Chem. B* **108**, 6673 (2004).
- ²⁴J. A. Torres, P. F. Nealey, and J. J. de Pablo, *Phys. Rev. Lett.* **85**, 3221 (2000).
- ²⁵R. J. Lang and D. S. Simmons, *Macromolecules* **46**, 9818 (2013); R. J. Lang, M. L. Merling, and D. S. Simmons, *ACS Macro Lett.* **3**, 758 (2014).
- ²⁶A. Shavit and R. A. Riddleman, *Macromolecules* **46**, 5044 (2014).
- ²⁷G. Adam and J. H. Gibbs, *J. Chem. Phys.* **43**, 139 (1965); K. F. Freed, *Acc. Chem. Res.* **44**, 194 (2011).
- ²⁸J. D. Stevenson and P. G. Wolynes, *J. Chem. Phys.* **129**, 234514 (2008).
- ²⁹P. Z. Hanakata, J. F. Douglas, and F. W. Starr, *Nat. Commun.* **5**, 4163 (2014); T. Salez, J. Salez, K. Dalnoki-Veress, E. Raphael, and J. A. Forrest, *Proc. Natl. Acad. Sci. U. S. A.* **112**, 8227 (2015).
- ³⁰S. Butler and P. Harrowell, *J. Chem. Phys.* **95**, 4454 (1991); D. Chandler and J. P. Garrahan, *Annu. Rev. Phys. Chem.* **61**, 191 (2010).
- ³¹J. E. G. Lipson and S. T. Milner, *Macromolecules* **43**, 9874 (2010); *Eur. Phys. B* **72**, 133 (2009); *Soft Matter* **9**, 9403 (2013).
- ³²S. Mirigian and K. S. Schweizer, *J. Phys. Chem. Lett.* **4**, 3648 (2013).
- ³³S. Mirigian and K. S. Schweizer, *J. Chem. Phys.* **140**, 194506 (2014).
- ³⁴S. Mirigian and K. S. Schweizer, *J. Chem. Phys.* **140**, 194507 (2014).
- ³⁵S. Mirigian and K. S. Schweizer, *Macromolecules* **48**, 1901 (2015).
- ³⁶S. Mirigian and K. S. Schweizer, *J. Chem. Phys.* **141**, 161103 (2014).
- ³⁷J. C. Dyre, *J. Non-Cryst. Solids* **235-237**, 142 (1998); *Rev. Mod. Phys.* **78**, 953 (2006).
- ³⁸F. Stikel, E. W. Fischer, and R. Richert, *J. Chem. Phys.* **102**(15), 6251 (1995).
- ³⁹M. Rubinstein and R. H. Colby, *Polymer Physics* (Oxford University Press, 2003).
- ⁴⁰Z. Yang, Y. Fujii, F. K. Lee, C. H. Lam, and O. K. C. Tsui, *Science* **328**, 1676 (2010).
- ⁴¹L. Zhu, C. W. Brian, S. F. Swallen, P. T. Straus, M. D. Ediger, and L. Yu, *Phys. Rev. Lett.* **106**, 256103 (2011); S. F. Swallen and M. D. Ediger, *Soft Matter* **7**, 10339 (2011).
- ⁴²W. Zhang, C. W. Brian, and L. Yu, *J. Phys. Chem. B* **119**, 5071 (2015); C. W. Brian and L. Yu, *J. Phys. Chem. A* **117**, 13303 (2013).
- ⁴³C. R. Daley, Z. Fakhraai, M. D. Ediger, and J. A. Forrest, *Soft Matter* **8**, 2206 (2012).
- ⁴⁴L. Yu, private communication (2015).
- ⁴⁵E. C. Glor and Z. Fakhraai, *J. Chem. Phys.* **141**, 194505 (2014).
- ⁴⁶E. C. Glor, R. J. Composto, and Z. Fakhraai, *Macromolecules* **48**, 6682 (2015).
- ⁴⁷J. E. Pye, K. A. Rohald, E. A. Baker, and C. B. Roth, *Macromolecules* **43**, 8296 (2010).
- ⁴⁸J. L. Keddie, R. A. L. Jones, and R. A. Cory, *Europhys. Lett.* **27**, 59 (1994).
- ⁴⁹M. D. Ediger, *Annu. Rev. Phys. Chem.* **51**, 99 (2000).
- ⁵⁰S. Mirigian and K. S. Schweizer, "Theory of elasticity, nonisothermal mobility gradients and chemical effects in free-standing films" (unpublished).
- ⁵¹C. Zhang, Y. Guo, and R. D. Priestly, *Macromolecules* **44**, 4001 (2011).
- ⁵²P. A. O'Connell, J. Wang, T. A. Ishola, and G. B. McKenna, *Macromolecules* **45**, 2453 (2012).